

Optimal active disturbance rejection control with applications in electric vehicles

Juan Quecan-Herrera¹, Sergio Rivera¹, Jorge Neira-García², John Cortés-Romero¹

¹Departamento de Ingeniería Eléctrica y Electrónica, Facultad de Ingeniería, Universidad Nacional de Colombia, Bogotá D.C., Colombia

²Polytechnic Institute, Purdue University, West Lafayette, USA

Article Info

Article history:

Received Dec 22, 2024

Revised Aug 30, 2025

Accepted Sep 10, 2025

Keywords:

Active disturbance rejection control

Induction motor

Metaheuristics

Nonlinear control

Optimization

ABSTRACT

This work proposes an optimal control strategy based on a modified active disturbance rejection control (ADRC) that considers disturbance weighting for a three-phase induction motor under rotor field-oriented control (FOC) to enhance energy efficiency. Induction motors (IMs) are widely used in electric vehicles (EVs) due to their cost-effectiveness and technological maturity. However, improving energy efficiency remains a key challenge, as it directly impacts vehicle range. The proposed approach employs ADRC, where part of the disturbance rejection task is handled offline by a hybrid optimization algorithm combining particle swarm optimization (PSO), tabu search (TS), and simulated annealing (SA) to tune a state-feedback controller. The controller parameters are optimized using a composite cost function that balances energy consumption and performance. Simulation and experimental results indicate that disturbance weighting has a significant impact on both problem complexity and performance. Optimal weighting improves the overall system response compared to conventional disturbance rejection methods. Energy and performance analyses show that disturbance weighting enhances energy usage compared to the traditional ADRC method, suggesting a novel efficiency control strategy for electric machines.

This is an open access article under the [CC BY-SA](https://creativecommons.org/licenses/by-sa/4.0/) license.



Corresponding Author:

Juan Quecan-Herrera

Departamento de Ingeniería Eléctrica y Electrónica, Facultad de Ingeniería

Universidad Nacional de Colombia

Bogotá D.C., Colombia

Email: jsquecanh@unal.edu.co

1. INTRODUCTION

Today, balancing economic development and environmental preservation is critical, particularly in the transportation sector, where internal combustion engines (ICEs) contribute to pollution. This has led to a growing focus on electric vehicles (EVs) as a cleaner alternative, driven by the need for energy efficiency and performance improvements [1]-[4]. Among the motor options for EVs, induction motors (IMs) are popular due to their robustness, cost-effectiveness, and high initial torque, despite limitations such as efficiency losses [5]-[9]. Control strategies like field-oriented control (FOC) are commonly used for IMs, offering independent control of rotor flux and torque [9].

This paper explores the role of optimal control theory in improving induction motor performance in EVs, focusing on active disturbance rejection control (ADRC) to handle unknown system disturbances [10], [11]. While traditional ADRC excels in performance, it does not address energy consumption, a critical factor for EV range. We propose a modified ADRC that incorporates disturbance weighting and use a hybrid metaheuristic algorithm combining particle swarm optimization (PSO), simulated annealing (SA), and tabu search (TS) to tune both control and disturbance rejection parameters [12], [13]. We identify several gaps in

the literature: traditional ADRC neglects energy use in disturbance rejection, and current control schemes often rely on conventional algorithms, overlooking newer or hybrid approaches. To improve performance, we propose using advanced methods to optimize ADRC parameters, with a specific focus on disturbance weighting [14]-[19]. This approach shows that disturbance weighting could improve the system's efficiency while maintaining robustness. Considering the above, our main contribution includes:

The implementation of a modified ADRC where disturbance weighting is considered, showing improved performance, and demonstrating that the disturbance weighting value depends on the chosen performance criteria. Simulation results compare the traditional ADRC with the modified version under the rotor FOC scheme, optimizing energy use and performance. Experimental results further validate the proposed control scheme.

This paper is structured as: section 2 reviews the method, briefly describing the dynamics of EVs and IMs under the FOC scheme, along with the problem statement and the optimal control design using a modified ADRC. Section 3 presents the results and discussion, including simulation outcomes and experimental findings. Section 4 concludes the paper.

2. METHOD

This section introduces the dynamics of EVs and IMs, outlines the control problem, and presents a case study using a hybrid algorithm for controller tuning.

2.1. Induction motor and electric vehicle dynamics

2.1.1 Vehicle dynamics

EVs dynamics involve forces such as rolling resistance (F_{ro}), aerodynamic drag (F_{ad}) and climbing resistance (F_{cr}), influencing road [20]-[22]. The total road load is expressed as:

$$F_{\omega} = F_{ro} + F_{ad} + F_{cr} + F_{sf} \quad (1)$$

where the forces are:

$$F_{ro} = \zeta mg \cos(\alpha), F_{ad} = \frac{1}{2} \pi K \omega F_A (v + v_0), F_{cr} = \pm mg \sin(\alpha), F_{sf} = k_A v \quad (2)$$

Here, m is the vehicle mass, g gravity, α the slope angle, and ζ depends on tire pressure and speed. K_{ω} is the drag coefficient, v_0 the headwind speed, v the vehicle speed, π air density, F_A the frontal area, and k_A Stokes' coefficient. F_{sf} is often negligible compared to F_{ro} . While the total motor torque $\tau_L(t)$ is:

$$\tau_L(t) = \tau_{fL}(t) + \frac{R_{\omega}}{G_r} + \tau_{TL}(t) \quad (3)$$

where $\tau_{TL}(t)$ relates to wheel torque, R_{ω} the wheel radius, G_r the transmission ratio, and τ_{fL} the shaft friction torque. The motor torque dynamic (4):

$$J_{EV} \frac{d\omega}{dt} = \tau_e(t) - \tau_L(t) \quad (4)$$

where $\tau_e(t)$ is motor torque, and J_{EV} is the total motor inertia:

$$J_{EV} = J + \frac{1}{2} \left(\frac{R_{\omega}}{G_r} \right)^2 m_{\omega} + \frac{1}{2} \left(\frac{R_{\omega}}{G_r} \right)^2 m(1 - s_{\omega}) \quad (5)$$

where J is motor inertia, m_{ω} the wheel mass, and s_{ω} wheel slippage.

2.1.2. Induction motor

IMs, widely used in EVs, are often controlled with rotor FOC [23], [24], leveraging Clarke (α/β scheme) and Park (d/q scheme) transformations:

$$\begin{bmatrix} s_d(t) \\ s_q(t) \end{bmatrix} = \begin{bmatrix} \cos(\rho(t)) & \sin(\rho(t)) \\ -\sin(\rho(t)) & \cos(\rho(t)) \end{bmatrix} \begin{bmatrix} s_{\alpha}(t) \\ s_{\beta}(t) \end{bmatrix}, \quad \rho = \tan^{-1} \left(\frac{\psi_{R\alpha}}{\psi_{R\beta}} \right), \quad \psi_d(t) = \sqrt{\psi_{R\alpha}(t)^2 + \psi_{R\beta}(t)^2} \quad (6)$$

where s represents the currents and voltages. Thus, the dynamic induction motor model under FOC scheme is:

$$\frac{d\theta(t)}{dt} = \omega(t) \quad (7)$$

$$\frac{d\omega(t)}{dt} = \mu\psi_d(t)i_q(t) - \frac{1}{J}\tau_L(t) \quad (8)$$

$$\frac{d\psi_d(t)}{dt} = -\eta\psi_d(t) + \eta Mi_d(t) \quad (9)$$

$$\frac{di_d(t)}{dt} = -\gamma i_d(t) + \frac{\eta M}{\sigma L_R L_S} \psi_d(t) + n_p \omega(t) i_q(t) + \frac{\eta M i_q^2(t)}{\psi_d(t)} + \frac{1}{\sigma L_S} u_d(t) \quad (10)$$

$$\frac{di_q(t)}{dt} = -\gamma i_q(t) + \frac{n_p M}{\sigma L_R L_S} \psi_d(t) - n_p \omega(t) i_d(t) + \frac{\eta M i_q(t) i_d(t)}{\psi_d(t)} + \frac{1}{\sigma L_S} u_q(t) \quad (11)$$

$$\frac{d\rho(t)}{dt} = n_p \omega(t) + \frac{\eta M i_d(t)}{\psi_d(t)} \quad (12)$$

The parameters are:

$$\eta = \frac{R_R}{L_R}, \quad \beta = \frac{M}{\sigma L_R L_S}, \quad \gamma = \frac{M^2 R_R}{\sigma L_R^2 L_S}, \quad \sigma = 1 - \frac{M^2}{L_R L_S}$$

Key variables include: rotor position (θ), angular speed (ω), load torque (τ_L), and magnetic flux (ψ_d). $u_d(t)$ and $u_q(t)$ represent voltages, while $i_d(t)$ and $i_q(t)$ are stator currents under d/q. R_R and R_S are rotor and stator resistances; L_R and L_S are rotor and stator inductances; M is magnetizing inductance and n_p the pole pair count. The FOC offers control over direct current ($i_d(t)$), quadrature current ($i_q(t)$), flux magnitude, and angular speed [25].

2.2. Problem statement and optimal control design

2.2.1. Problem statement

Considering the dynamics of the induction motor and its control using ADRC, the following performance criterion is proposed:

$$J = \int_{t_0}^{t_f} (K_1 P(t) + K_2 e(t) + K_3 t_{sc}(t)) dt, \quad s.t. \quad g_i(x) \leq a_i, \quad i \in \{1, 2, 3, \dots, n\}, \quad a_i \in R. \quad (13)$$

In (14), $P(t)$ represents the motor's power consumption, calculated as the sum of the absolute values of the product of currents and voltages under the two-phase α/β scheme using Clarke's transformation. The term $e(t)$ denotes the angular speed tracking error, and $t_{sc}(t)$ represents the settling time, weighted by the operation time. The weights K_1 , K_2 and K_3 balance the relative importance of these components. To improve the performance of control laws, it is essential to address the limitations of current ADRC methods. While parameter tuning in ADRC using optimization algorithms enhances performance, it often overlooks energy efficiency. This highlights the need for a new ADRC-based control scheme that explicitly incorporates energy consumption considerations.

– Global optimum in ADRC approach - motivational example

Consider the nonlinear system:

$$\dot{x}_1(t) = \lambda x_1(t), \quad \dot{x}_2(t) = \beta x_1^2(t) + \alpha x_2(t) + \zeta u(t), \quad \{\beta, \alpha, \zeta, \lambda\} \in R, \quad (14)$$

where $\lambda \in R^-$ ensures stability. For $\lambda = -1$ and $\zeta = \alpha = \beta = 1$, under ADRC, the system becomes:

$$\dot{x}_2(t) = x_1^2(t) + x_2(t) + u(t) \rightarrow \dot{y} = \kappa u(t) + \xi(t), \quad (15)$$

with $\xi(t) = x_1^2(t) + x_2(t)$ where $\kappa = 1$. The disturbance dynamics are $\dot{\xi}(t) = -\xi(t) + 2x_2(t) + u(t)$. Thus, the extended system dynamics, considering the disturbance model, are:

$$\begin{bmatrix} \dot{x}_1(t) \\ \dot{x}_2(t) \\ \dot{\xi}(t) \end{bmatrix} = \begin{bmatrix} -1 & 0 & 0 \\ 0 & 0 & 1 \\ 0 & 2 & -1 \end{bmatrix} \begin{bmatrix} x_1(t) \\ x_2(t) \\ \xi(t) \end{bmatrix} + \begin{bmatrix} 0 \\ 1 \\ 1 \end{bmatrix} u(t). \quad (16)$$

Using a linear quadratic regulator (LQR) framework, the optimal control gains are:

$$k = -[0 \quad 1.707 \quad 0.07071]. \quad (17)$$

The resulting control law is $u(t) = -1.707x_2(t) - 0.07071 \xi(t)$. This demonstrates that the disturbance should not be fully rejected for optimal performance. Consequently, this research proposes the control strategy shown in Figure 1, which incorporates disturbance weighting in the ADRC scheme:

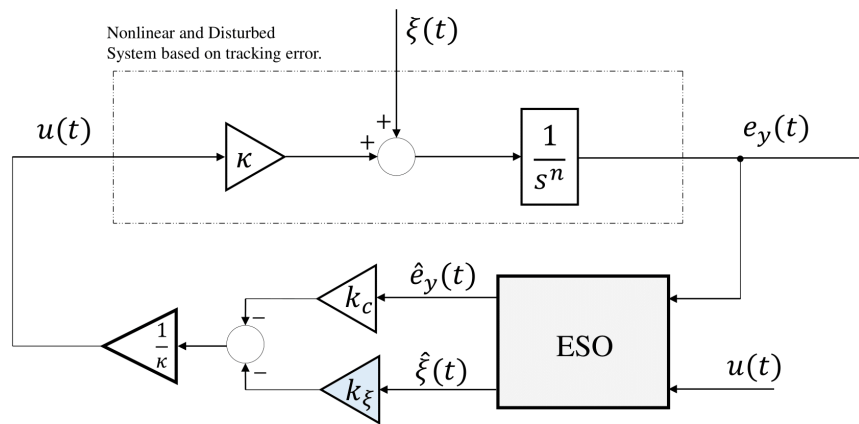


Figure 1. Proposed control strategy

The proposed strategy includes disturbance weighting via parameter k_ξ and stability gain tuning through k_c achieved via error state feedback. To optimize both disturbance weighting and controller parameters effectively, an optimization algorithm is required.

– Hybrid algorithm

A hybrid algorithm is employed in this research due to the complexity of the problem. The algorithm is composed of three sub-algorithms: The PSO algorithm, TS, and SA. The algorithm diagram is shown in Figure 2.

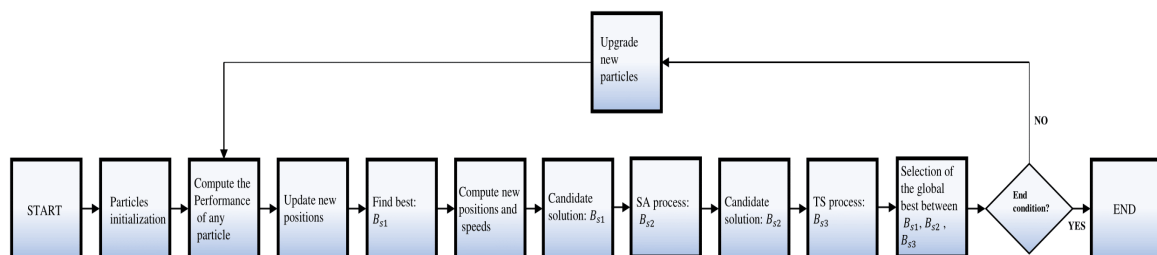


Figure 2. Hybrid algorithm scheme

Particles initialization: in this step, the particles of the traditional PSO algorithm are initialized.

Compute the performance of any particle: the performance of each particle is computed based on a predefined performance criterion.

Update new positions: new positions are computed following the traditional PSO scheme.

Find best: B_{s1} : the best particle is selected.

Compute new positions and speeds: all new positions and speeds are computed considering the particles updated information.

Candidate solution: B_{s1} : the best solution from the PSO algorithm, B_{s1} , is used as the initial solution for the SA algorithm.

SA process: B_{s2} : the SA algorithm processes the initial solution and produces a new best solution, B_{s2} .

Candidate solution: B_{s2} : the best solution from the SA algorithm, B_{s2} , is used as the candidate solution for the TS algorithm.

TS process: B_{s3} : the TS algorithm processes the candidate solution and produces a new best solution, B_{s3} .

Selection of the global best between B_{s1} , B_{s2} , B_{s3} : the best solution is selected from B_{s1} , B_{s2} and B_{s3} . If the termination condition is not met, the algorithm is repeated.

– Control design

The control design considers the dynamics of angular speed, direct current, and quadrature current within the framework of ADRC, based on the system dynamics from Section 2.1.2.

$$\frac{d\omega(t)}{dt} = \mu\psi_d(t)i_q(t) + \xi_{\omega 1}(t), \frac{di_d(t)}{dt} = \frac{1}{\sigma L_s}u_d(t) + \xi_{id1}(t), \frac{di_q(t)}{dt} = \frac{1}{\sigma L_s}u_q(t) + \xi_{iq1}(t) \quad (18)$$

where $\xi_{\omega 1}(t)$, $\xi_{id1}(t)$ and $\xi_{iq1}(t)$ represent unified disturbances for each controlled variable. These dynamics are simplified as first-order systems for control design:

$$\frac{dy(t)}{dt} = \kappa u(t) + \xi(t) \quad (19)$$

where $y(t)$ is the output, $u(t)$ the control signal, κ an average value, and $\xi(t)$ the unified disturbance. By introducing the tracking error $e_y(t) = y(t) - y^*(t)$ and using an internal model assuming constant disturbance, the extended state is defined as $x_1(t) = e_y(t)$ and $x_2(t) = \xi(t)$, leading to the state-space dynamics:

$$\begin{bmatrix} \dot{x}_1(t) \\ \dot{x}_2(t) \end{bmatrix} = \begin{bmatrix} 0 & 1 \\ 0 & 0 \end{bmatrix} \begin{bmatrix} x_1(t) \\ x_2(t) \end{bmatrix} + \begin{bmatrix} \kappa \\ 0 \end{bmatrix} u(t) + \begin{bmatrix} 0 \\ 1 \end{bmatrix} \xi(t) \quad (20)$$

with the output:

$$x_1(t) = e_y(t) = \begin{bmatrix} 1 & 0 \end{bmatrix} \begin{bmatrix} x_1(t) \\ x_2(t) \end{bmatrix} \quad (21)$$

using the extended state observer (ESO), the estimated states ($\hat{e}_y(t)$ and $\hat{\xi}(t)$) facilitate the control law for each variable. For angular speed:

$$\frac{de_{\omega}(t)}{dt} = \mu\psi_d(t)u_{\omega}(t) + \xi_{\omega}(t) \quad (22)$$

with the control law:

$$u_{\omega}(t) = \frac{1}{\mu\psi_d(t)} (-k_{\omega} \hat{e}_{\omega}(t) - k_{\xi\omega} \hat{\xi}_{\omega}(t)) \quad (23)$$

Substituting into the dynamics and expressing in the laplace domain:

$$(s + k_{\omega})e_{\omega}(s) = (1 - k_{\xi\omega})\xi_{\omega}(s) - k_{\xi\omega}\Delta \xi_{\omega}(s) - k_{\omega}\Delta e_{\omega}(s) \quad (24)$$

where k_{ω} manages stability, $k_{\xi\omega}$ regulates tracking performance, and Δ represents the estimation error. While for the direct current dynamics:

$$\frac{de_{id}(t)}{dt} = \frac{1}{\sigma L_s}u_{id}(t) + \xi_{id}(t) \quad (25)$$

the control law is:

$$u_{id}(t) = \sigma L_s (-k_{id} \hat{e}_{id}(t) - k_{\xi id} \hat{\xi}_{id}(t)) \quad (26)$$

leading to similar stability and performance trade-offs as angular speed. The quadrature current control follows analogous principles. In summary, $k_{\xi id}$, $k_{\xi iq}$, and $k_{\xi \omega}$ represent disturbance weighting parameters, while k_{id} , k_{iq} , and k_{ω} manage stability. To simplify optimization and maintain linearity, $k_{\xi \omega} = 1$ is selected. Figure 3 illustrates the induction motor under the FOC scheme, where the proposed hybrid algorithm is used for offline optimization.

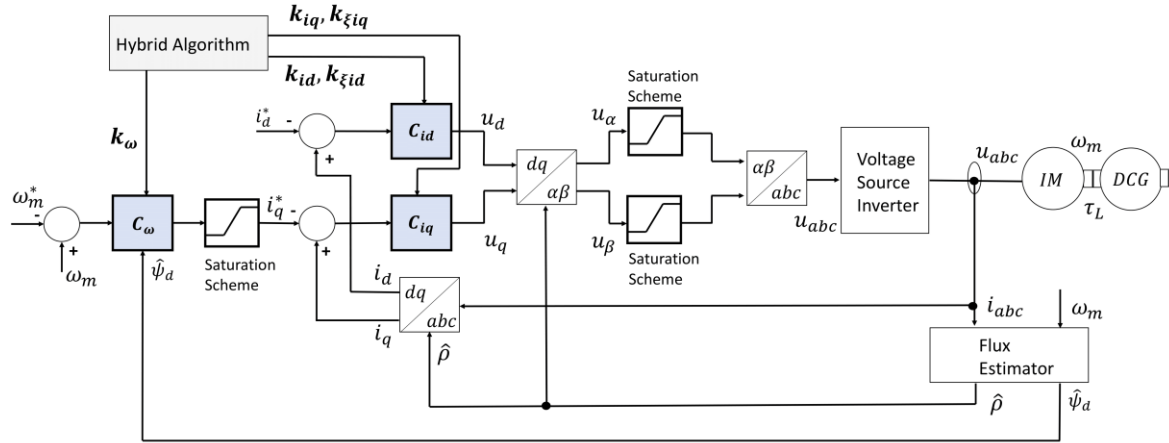


Figure 3. Proposed control scheme

The controllers C_{id} , C_{iq} and C_ω , based on the Figure 3, incorporate flux estimators for the rotor FOC scheme:

$$\frac{d\hat{\psi}_d(t)}{dt} = -\eta \hat{\psi}_d(t) + \eta M i_d(t), \quad \frac{d\hat{\rho}(t)}{dt} = -n_p \omega(t) + \eta M \frac{i_q(t)}{\hat{\psi}_d(t)} \quad (27)$$

A saturation scheme ensures the control signal remains within practical bounds, while offline simulation determines disturbance weighting parameters and evaluates the vehicle dynamics through a direct current (DC) generator.

– Induction of motor and vehicle parameters

Details the parameters of the induction motor and the electric vehicle: the nominal speed per pole pair is 1500 rpm, operating at 70 V and 50 Hz with a nominal current of 1.2 A. The stator and rotor resistances are 6.575 Ω and 19.577 Ω , respectively. The nominal torque is 0.6 Nm, and the nominal power is 100 W. The motor's magnetization inductance is 243.4 mH, while the rotor and stator leakage inductances are 5.4 mH and 55.2 mH, respectively. Regarding the vehicle, its mass is 98 Kg, with a wheel radius of 0.3594 m and a fixed gear ratio of 9.73. The frontal area measures 2.4 m^2 and the air density is 1.1839 $\frac{kg}{m^3}$. The aerodynamic drag coefficient is 0.24, the rolling resistance coefficient is 0.002, and γ is 5.3475.

3. RESULTS AND DISCUSSION

This section presents simulation and experimental results. The disturbance weighting is determined through the simulation results, and the parameter tuning is validated through the experimental results.

3.1. Simulation results

3.1.1. Reference considered

This subsection presents an analysis using the hybrid algorithm under offline simulation. It compares traditional ADRC with a modified ADRC based on disturbance weighting. The reference used in the optimization problems is shown in Figure 4 and is based on the urban dynamometer driving schedule (UDDS), commonly used in electric vehicle tests.

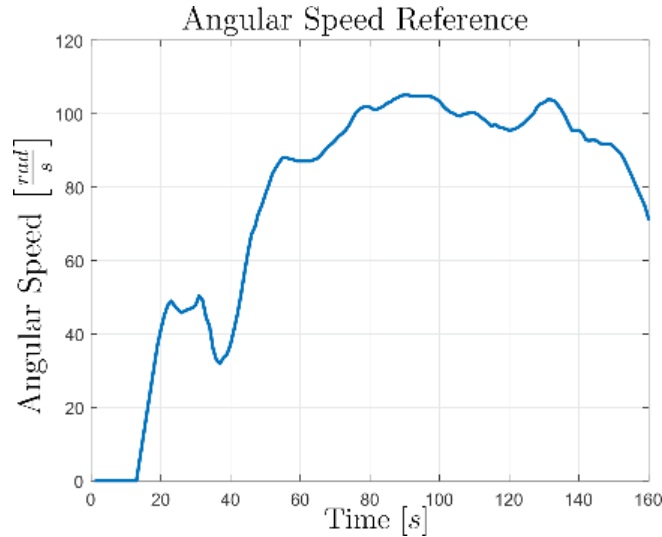


Figure 4. Reference for the optimization problems

The weighting parameters for the cost function J were selected through simulation tests. The comparison between the traditional ADRC and the modified version was based on the following optimization problems.

3.1.2. ADRC (disturbance rejection)

$$J = \int_0^{160} (0.35P(t) + 50e(t) + 500t_{sc}(t))dt. \quad (28)$$

S.t $60 \leq k_\omega \leq 300, 60 \leq k_{id} \leq 300, 60 \leq k_{iq} \leq 300$.

The objective of the first optimization problem is to tune the parameters of the control law to guarantee the stability of the system. In this case, disturbance weighting is not considered, in other words $k_{\xi iq} = k_{\xi id} = k_{\xi \omega} = 1$.

3.1.3. Modified ADRC (disturbance weighting)

For this case, the optimization problem is given by:

$$J = \int_0^{160} (0.35P(t) + 50e(t) + 500t_{sc}(t))dt. \quad (29)$$

$$\text{S.t } 60 \leq k_\omega \leq 300, 60 \leq k_{id} \leq 300, 60 \leq k_{iq} \leq 300, 0.990 \leq k_{\xi iq} \leq 1.1, 0.990 \leq k_{\xi id} \leq 1.1.$$

In this case, the disturbance weighting for the currents is considered, and the constraints of all variables for both optimization problems are related to the ADRC capabilities and numerical stability.

3.1.4. Results of the first comparison analysis

Parameters for the hybrid algorithm used to tune control strategies. For tuning k_{id} , k_{iq} , and k_ω in disturbance rejection, three variables are optimized with limits ranging from 60 to 300. The algorithm employs 10 particles and a maximum of 30 iterations, with C_1 and C_2 set to 0.7, and inertia weights W_{max} and W_{min} at 0.9 and 0.2, respectively. The initial temperature is 10 or 5, with an annealing rate of 0.7. A tabu list of length 10, a neighborhood size of 3, and 3 TS iterations are also used. For tuning k_{id} , k_{iq} , k_ω , $k_{\xi id}$, and $k_{\xi iq}$, five variables are optimized with limits from (60, 60, 60, 0.990, 0.990) to (300, 300, 300, 1.1, 1.1), using the same setup. The initial temperature is adjusted depending on the current temperature and the comparison between PSO and hybrid performance: if the temperature is 1 or the hybrid algorithm outperforms PSO, the new initial temperature is set to 5 to refine the search space. Considering the results, disturbance weighting demonstrates better performance compared to disturbance rejection, although the number of iterations suggests that it may involve higher complexity, as further detailed in Table 1.

Table 1. Results of tuning-disturbance rejection and disturbance weighting

Variable	Disturbance weighting	Disturbance rejection
k_{ld}	71.0542	60
k_{lq}	300	300
k_{ω}	300	300
$k_{\xi ld}$	1.0273	Not considered
$k_{\xi lq}$	1.1	Not considered
Number of iterations	23	3

3.2. Experimental results

3.2.1. Experimental conditions

The following conditions were taken into account for the experiment:

- In this research experiment, the system's slope is disregarded, and the dynamics are modeled using a DC motor. The objective is to model the machine's current reference to describe the torque. Consequently, the climbing force is not considered, meaning $\alpha = 0$ (the road slope angle is ignored), and F_{sf} is excluded (as per (1)).
- For the ESO design in the induction motor, the eigenvalues associated with the currents are located at -650 and the eigenvalues for the speed are located at -610.
- The reference for the direct current is set to a constant value of $i_d^*(t) = 1.2[\text{A}]$.

3.2.2. Experimental setup

This subsection details the experimental implementation of control strategies, involving a global experiment comparing two control strategies: one focused on disturbance rejection and the other on disturbance weighting, with each strategy undergoing ten trials to mitigate uncertainties in measurement equipment and motor conditions. The system's angular speed response is averaged, and the cost and standard deviation of both strategies are compared.

The experimental setup includes an induction motor, an XPC target for real-time control, a three-phase rectifier, three-phase inverter, DC-DC converter, and measurement systems for voltages and currents. The system operates by connecting a three-phase source to a VARIAC, which feeds a rectifier supplying DC voltage to an inverter controlled by pulse width modulation (PWM) signals through the XPC target. The inverter's output, filtered by an inductor-capacitor (LC) filter, drives an induction motor connected to a DC motor that acts as a load, with the DC motor's current regulated by a DC-DC converter. The entire setup, including measurement instruments and control signals, is managed in real-time using MATLAB, with components interconnected through a transmission control protocol/internet protocol (TCP/IP). The experimental setup is illustrated in Figure 5.

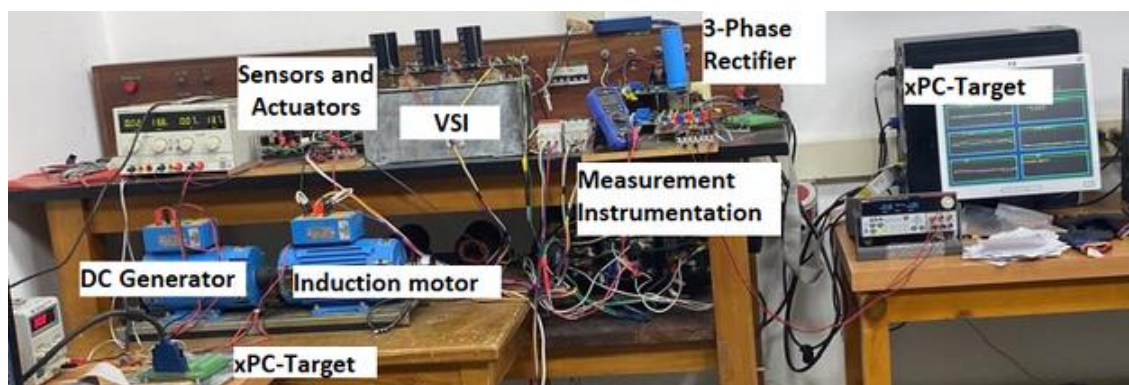


Figure 5. Experimental setup

3.2.3. Experimental results

In this subsection, the experimental setup of Figure 5 was used using the control parameters listed in Table 1. A comparison between the traditional ADRC and the modified version was made using different performance criteria. Results show the modified version outperforms the traditional ADRC.

– Reference and experimental setup

The experiment evaluates vehicle performance under urban conditions using the UDDS driving cycle, depicted as Figure 6(a). This cycle simulates typical urban scenarios. Ten trials per strategy are conducted to reduce uncertainties from measurement noise and communication protocols. The analysis includes disturbance rejection and disturbance weighting strategies, focusing on energy use, performance, and cost variations.

– Comparison analysis

Table 1 lists the parameters for implementations. Figures 6(a) and (b) show the arithmetic mean (AM) of angular speed response and costs for both strategies. Disturbance weighting shows greater variability but higher overall performance, while disturbance rejection incurs higher costs, showing that disturbance weighting can improve the performance of the disturbance rejection algorithm. Additionally, energy and performance are evaluated using parameters ($E_m(t)$) and ($E_p(t)$), defined as

$$E_m(t) = \int_{t_0}^{t_f} (p_m(\tau)) d\tau, \quad E_p(t) = \int_{t_0}^{t_f} (|e_m(\tau)| p_m(\tau)) d\tau, \quad (30)$$

where $p_m(t)$ represents power, and $e_m(t)$ is the tracking error. Figures 6(c) and (d) illustrate these parameters, showing better performance for the disturbance weighting strategy. To assess cost variation, parameter R is used, where $R = \left(\frac{\text{Arithmetic mean of costs}}{\text{Standard deviation of costs}} \right)$. For the disturbance rejection case the parameter R is equal to 4.788, while for the disturbance weighting case the value is equal to 9.804, showing higher cost variability for disturbance weighting due to its nonlinear control scheme.

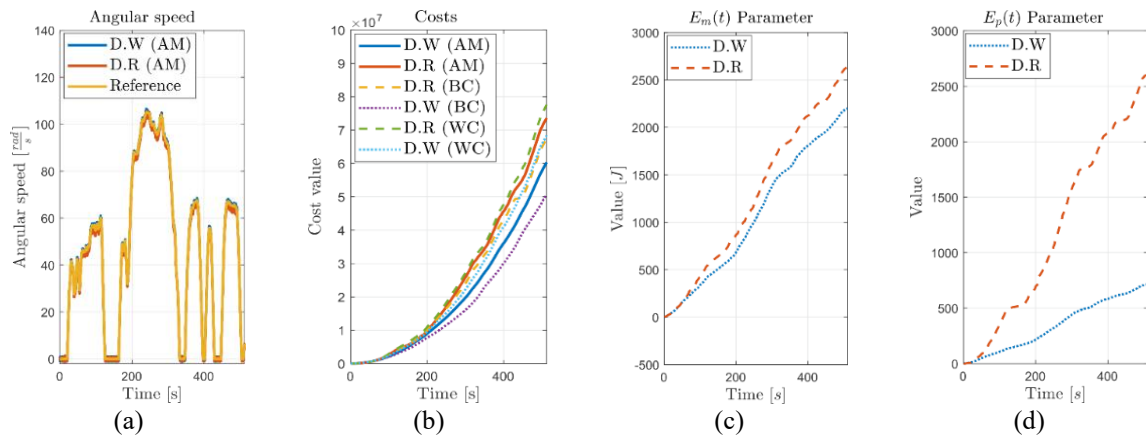


Figure 6. Experimental results; (a) angular speed comparison, (b) cost comparison, (c) E_m parameter, and (d) E_p parameter

4. CONCLUSION

IMs are widely used in EVs due to their robustness and efficiency. However, vehicle range remains a critical concern. This work proposed a modified ADRC approach, incorporating a disturbance weighting factor and tuning its parameters through a metaheuristic algorithm. This method demonstrated improved performance compared to traditional techniques. Nevertheless, the increased complexity of the problem may limit the capabilities of conventional ADRC, especially when complete disturbance rejection is not achieved. As a result, the disturbance weighting factor was designed to remain close to one, accounting for system uncertainties and the nonlinear dynamics of the induction motor. However, this strategy represents a new opportunity for ADRC-related optimization problems because the traditional methodology does not consider the impact of incorporating control flexibility into the design because the methodology assumes perfect disturbance rejection. For future work, it is recommended to extend this approach to other types of motors, integrating disturbance weighting strategies with alternative metaheuristic algorithms commonly found in the literature to validate its generalizability and performance across different motor drive systems.

ACKNOWLEDGEMENTS

The authors would like to thank the Universidad Nacional de Colombia for their support.

FUNDING INFORMATION

This research was supported by the Universidad Nacional de Colombia, which provided funding for the acquisition and use of the equipment employed in this project.

AUTHOR CONTRIBUTIONS STATEMENT

This journal uses the Contributor Roles Taxonomy (CRediT) to recognize individual author contributions, reduce authorship disputes, and facilitate collaboration.

Name of Author	C	M	So	Va	Fo	I	R	D	O	E	Vi	Su	P	Fu
Juan Quecan-Herrera	✓	✓	✓	✓	✓	✓		✓	✓	✓			✓	
Sergio Rivera		✓	✓			✓	✓			✓	✓	✓	✓	✓
Jorge Neira-García		✓	✓			✓				✓		✓	✓	
John Cortés-Romero	✓	✓			✓	✓	✓			✓		✓	✓	✓

C : **C**onceptualization

M : **M**ethodology

So : **S**oftware

Va : **V**alidation

Fo : **F**ormal analysis

I : **I**nterpretation

R : **R**esources

D : **D**ata Curation

O : **O**riginal Draft

E : **E**diting

Vi : **V**isualization

Su : **S**upervision

P : **P**roject administration

Fu : **F**unding acquisition

CONFLICT OF INTEREST STATEMENT

The authors declare that they have no known competing financial interests or personal relationships that could have appeared to influence the work reported in this paper.

INFORMED CONSENT

Not applicable.

ETHICAL APPROVAL

Not applicable.

DATA AVAILABILITY

The authors confirm that the data supporting the findings of this study are available within the article.




REFERENCES

- [1] C. Rao and B. Yan, "Study on the interactive influence between economic growth and environmental pollution," *Environmental Science and Pollution Research*, vol. 27, no. 31, pp. 39442–39465, 2020, doi: 10.1007/s11356-020-10017-6.
- [2] M. A. Hannan, M. M. Hoque, A. Hussain, Y. Yusof and P. J. Ker, "State-of-the-art and energy management system of lithium-ion batteries in electric vehicle applications: issues and recommendations," in *IEEE Access*, vol. 6, pp. 19362–19378, 2018, doi: 10.1109/ACCESS.2018.2817655.
- [3] S. Gnanavendan *et al.*, "Challenges, solutions and future trends in EV-technology: A review," *IEEE Access*, vol. 12, pp. 17242–17260, 2024, doi: 10.1109/ACCESS.2024.3353378.
- [4] Y. Balali and S. Stegen, "Review of energy storage systems for vehicles based on technology, environmental impacts, and costs," *Renewable and Sustainable Energy Reviews*, vol. 135, p. 110185, 2021, doi: 10.1016/j.rser.2020.110185.
- [5] M. Ismail, B. Elhady, and A. Bendary, "Variable voltage control of three-phase induction motor for energy saving," (*ERJ Engineering Research Journal*), vol. 44, no. 4, pp. 377–383, 2021, doi: 10.21608/erjm.2021.74659.1093.
- [6] D. Mohanraj, J. Gopalakrishnan, B. Chokkalingam and L. Mihet-Popa, "Critical aspects of electric motor drive controllers and mitigation of torque ripple-review," in *IEEE Access*, vol. 10, pp. 73635–73674, 2022, doi: 10.1109/ACCESS.2022.3187515.
- [7] S. Thangavel, D. Mohanraj, T. Girijaprasanna, S. Raju, C. Dhanamjayulu and S. M. Muyeen, "A comprehensive review on electric vehicle: battery management system, charging station, traction motors," in *IEEE Access*, vol. 11, pp. 20994–21019, 2023, doi: 10.1109/ACCESS.2023.3250221.
- [8] A. Rehman, R. Ghias, I. Ahmad, and H. I. Sherazi, "Advanced nonlinear controller for hybrid energy storage system integrated with three-phase induction motor in hybrid electric vehicles," *Journal of Energy Storage*, vol. 131, no. PA, p. 117388, 2025, doi: 10.1016/j.est.2025.117388.
- [9] C. Liu, K. T. Chau, C. H. T. Lee and Z. Song, "A critical review of advanced electric machines and control strategies for electric vehicles," in *Proceedings of the IEEE*, vol. 109, no. 6, pp. 1004–1028, June 2021, doi: 10.1109/JPROC.2020.3041417.
- [10] H. Sira-Ramírez and S. K. Agrawal, "Differentially Flat Systems," *CRC Press*, 1st ed. Marcel Dekker, Inc., 2004, doi: 10.1201/9781482276640.




- [11] Z. Gao, "Active disturbance rejection control: a paradigm shift in feedback control system design," *2006 American Control Conference, Minneapolis, MN, USA, 2006*, pp. 7 pp.-, doi: 10.1109/ACC.2006.1656579.
- [12] Z. Yin, C. Du, J. Liu, X. Sun and Y. Zhong, "Research on auto disturbance-rejection control of induction motors based on an ant colony optimization algorithm," in *IEEE Transactions on Industrial Electronics*, vol. 65, no. 4, pp. 3077-3094, April 2018, doi: 10.1109/TIE.2017.2751008.
- [13] C. Du, Z. Yin, Y. Zhang, J. Liu, X. Sun and Y. Zhong, "Research on active disturbance rejection control with parameter autotune mechanism for induction motors based on adaptive particle swarm optimization algorithm with dynamic inertia weight," in *IEEE Transactions on Power Electronics*, vol. 34, no. 3, pp. 2841-2855, March 2019, doi: 10.1109/TPEL.2018.2841869.
- [14] W. Cai, J. Yang, Y. Yu, Y. Song, T. Zhou and J. Qin, "PSO-ELM: A hybrid learning model for short-term traffic flow forecasting," in *IEEE Access*, vol. 8, pp. 6505-6514, 2020, doi: 10.1109/ACCESS.2019.2963784.
- [15] M. A. Memon, M. D. Siddique, S. Mekhilef and M. Mubin, "Asynchronous particle swarm optimization-genetic algorithm (APSO-GA) based selective harmonic elimination in a cascaded h-bridge multilevel inverter," in *IEEE Transactions on Industrial Electronics*, vol. 69, no. 2, pp. 1477-1487, Feb. 2022, doi: 10.1109/TIE.2021.3060645.
- [16] Y. Wang, D. Wang and Y. Tang, "Clustered hybrid wind power prediction model based on ARMA, PSO-SVM, and clustering methods," in *IEEE Access*, vol. 8, pp. 17071-17079, 2020, doi: 10.1109/ACCESS.2020.2968390.
- [17] K. Jagatheesan, B. Anand, S. Samanta, N. Dey, A. S. Ashour and V. E. Balas, "Design of a proportional-integral-derivative controller for an automatic generation control of multi-area power thermal systems using firefly algorithm," in *IEEE/CAA Journal of Automatica Sinica*, vol. 6, no. 2, pp. 503-515, March 2019, doi: 10.1109/JAS.2017.7510436.
- [18] A. K. Mishra, S. R. Das, P. K. Ray, R. K. Mallick, A. Mohanty and D. K. Mishra, "PSO-GWO optimized fractional order PID based hybrid shunt active power filter for power quality improvements," in *IEEE Access*, vol. 8, pp. 74497-74512, 2020, doi: 10.1109/ACCESS.2020.2988611.
- [19] Z. Qi, Q. Shi and H. Zhang, "Tuning of digital PID controllers using particle swarm optimization algorithm for a CAN-based DC motor subject to stochastic delays," in *IEEE Transactions on Industrial Electronics*, vol. 67, no. 7, pp. 5637-5646, July 2020, doi: 10.1109/TIE.2019.2934030.
- [20] A. Haddoun, M. E. H. Benbouzid, D. Diallo, R. Abdessemed, J. Ghouili, and K. Srairi, "A loss-minimization DTC scheme for EV induction motors," in *IEEE Transactions on Vehicular Technology*, vol. 56, no. 1, pp. 81-88, Jan. 2007, doi: 10.1109/TVT.2006.889562.
- [21] G. Park, S. Lee, S. Jin, and S. Kwak, "Integrated modeling and analysis of dynamics for electric vehicle powertrains," *Expert Systems with Applications*, vol. 41, no. 5, pp. 2595-2607, 2014, doi: 10.1016/j.eswa.2013.10.007.
- [22] J. Neira-García, A. Beltrán-Pulido, and J. Cortés-Romero, "Algebraic speed estimation for sensorless induction motor control: insights from an electric vehicle drive cycle," *Electronics (Switzerland)*, vol. 13, no. 10, pp. 1-20, 2024, doi: 10.3390/electronics13101937.
- [23] M. Swargiary, J. Dey, and T. K. Saha, "Optimal speed control of induction motor based on linear quadratic regulator theory," *2015 Annual IEEE India Conference (INDICON)*, New Delhi, India, 2015, pp. 1-6, doi: 10.1109/INDICON.2015.7443806.
- [24] Š. Janouš, J. Talla, V. Šmídl and Z. Peroutka, "Constrained LQR control of dual induction motor single inverter drive," in *IEEE Transactions on Industrial Electronics*, vol. 68, no. 7, pp. 5548-5558, July 2021, doi: 10.1109/TIE.2020.2994885.
- [25] J. Chiasson, "Modeling and High-Performance Control of Electric Machines," *New York: John Wiley & Sons, Inc.*, 2005, doi: 10.1002/0471722359.

BIOGRAPHIES OF AUTHORS






Juan Quecan-Herrera    received a B.Sc. degree in Electronic Engineering in 2022 and M.S. degree in Industrial Automation in 2024, both from Universidad Nacional de Colombia. He is currently pursuing a Ph.D. Program in Sciences with a specialty in Automatic Control at the CINVESTAV Institute in Mexico. He is interested in and conducts research on tuning the parameters of advanced controllers using metaheuristic algorithms and deterministic methods. He can be contacted at email: jsquecanh@unal.edu.co.






Sergio Rivera    he is an Associate Professor in the Department of Electrical and Electronic Engineering of the Faculty of Engineering at the Universidad Nacional de Colombia, leading the Applied Computational Intelligence for the Electrical Sector group within the EMC-UN research group. He has served as Director of the Department (2023-2024) and coordinated the Master's and Doctorate programs in Electrical Engineering (2018-2022) at the same institution. He has been invited as a professor and researcher at the Karlsruhe Institute of Technology - KIT (Helmholtz Visiting Researcher Grant, HIDA), the University of Florida (Fulbright Scholar Grant, Visiting Scientist), the Technical University of Dortmund (Gambirous Fellowship and DAAD Research Stay Grant), and Ruhr University (VIP Program, Visiting International Professor). He completed postdoctoral research in the control and coordination of smart grids and microgrids at the Massachusetts Institute of Technology (MIT) and the Masdar Institute of Science and Technology, Khalifa University. He can be contacted at email: sriverar@unal.edu.co.



Jorge Enrique Neira-Garcia    he received his B.S. degree in Electrical Engineering (2018) and M.S. degree in Industrial Automation (2022) from Universidad Nacional de Colombia, Bogotá, Colombia. He is currently pursuing a Ph.D. in Technology at Purdue University, West Lafayette, IN, USA. His research focuses on integrating technology with meaningful social impact. His work spans assistive robotics, electric vehicle technologies, and sustainable energy. He combines active disturbance rejection control (ADRC), and algebraic identification/estimation methods with practical applications that enhance quality of life. His research contributions include novel approaches to robotic 2-DOF ankle-foot prosthesis design, sensor less induction motor control, and photovoltaic modeling. He can be contacted at email: jneiraga@purdue.edu.



John Cortés-Romero    he holds a degree in Electrical Engineering, a Master's in Industrial Automation, and a Master's in Mathematics from the Universidad Nacional de Colombia (1995, 1999, and 2007, respectively). He earned a Ph.D. in Science with a specialization in Electrical-Mechatronic Engineering from the CINVESTAV Institute in Mexico in 2011. He is currently a professor in the Department of Electrical and Electronic Engineering at the Universidad Nacional de Colombia. He can be contacted at email: jacortesr@unal.edu.co.